Development of areal-level individualized homologous functional parcellations in youth

Check for updates

Jinlong Li[1], Yu Zhang [1], Xinyu Wu[1], Mufan Xue[1], Zhiming Wang[1], Shuo Lv[1], Ruoqi Yang[1], Wenjing Zhu[1], Xuesong Li[2], Tianyi Yan [3] ✉ & Guoyuan Yang [1,3] ✉

Individualized functional brain networks from childhood to adolescence undergo varying patterns of maturation, associated with higher-order cognition outcomes. However, the developmental trajectory patterns based on homologous areal-level brain parcellations remain elusive. Here, we developed an individualized homologous functional parcellation technique (IHFP) to map brain functional development using resting-state functional magnetic resonance imaging data from the Lifespan Human Connectome Project in Development study ($N = 591$) aged 8–21 years. We delineate developmental trajectories based on areal-level homologous parcellations of resting-state functional connectivity. We found functional features during adolescence exhibit unique developmental trajectories, such as global mean functional connectivity with a widespread decrease across cerebral cortex. Then, we matched areal-level parcellations into large-scale networks and demonstrated that higher-order transmodal networks exhibited higher variability between developmental trajectories in areal-level parcels. We reveal that IHFPs possess a stronger capability for creating more homogeneous parcels in individuals, consequently showing a higher accuracy in predicting cognition behaviors. Together, these results establish the fine-grained areal-level functional homologous parcellations in adolescent development and will facilitate the understanding of human brain function more precisely.

Imaging-based parcellation, delineation of functional brain areas and networks that present a highly heterogeneous landscape[1,2], is fundamental for understanding brain organization and function from person to person[3–6]. Given that stable topology associated with individual cognitive abilities and behaviors, brain parcellation has been widely used in the field of neurodevelopment[7,8] and clinical applications[9,10]. So far, most neurodevelopmental studies based on homologous functional brain area have shown cortical developmental progresses are unique in adolescence, which is characterized by the maturation of cognitive, affective, and social processes[8,11,12]. However, typical research on adolescent brain development with individualized functional atlas mainly focus on large-scale networks[13–16], remaining gaps in fine-grained individualized homologous parcellations. Beyond large-scale networks, numerous fine-grained areal-level parcellation atlases have been proposed in group-level[17–22]. Even though existing group-level parcellation at finer scales allow for regional correspondence, this correspondence is limited to labels and does not account for functional or spatial information. Furthermore, due to substantial intersubject variability, establishing

functional homology at finer scales remains a major challenge[23]. As a result, normative developmental trajectories at the fine-grained areal-level remain poorly understood. Compared to group-level approaches, individualized parcellations may offer greater sensitivity in capturing subject-specific features[24,25].

Previous studies of large-scale brain networks have provided functional insights into spatiotemporal maturation of functional regions across the cortex. For example, functional topography in association cortex is most variable and refined with age[14]. Yet, the homogeneity of developmental trajectories in the association cortex and its relationship with individual cognitive abilities remain unclear at a fine-grained areal-level[9,18,25]. Areal-level individual parcellations can correspond with more precision to cortical areas and physiological features[19,20]. Related to this, various sites partaking in the default mode network (DMN) function could be further subdivided into functionally distinct subcomponents by the coactivation pattern with the rest of the brain[21,22]. Recently, Sun et al.[15] established the normative growth charts of functional brain connectome of system-level brain atlases across

[1]School of Interdisciplinary Science, Beijing Institute of Technology, Beijing, China. [2]School of Computer Science and Technology, Beijing Institute of Technology, Beijing, China. [3]School of Medical Technology, Beijing Institute of Technology, Beijing, China. ✉e-mail: yantianyi@bit.edu.cn; yanggy@bit.edu.cn

lifespan. However, studies of adolescent development with fine-grained areal-level brain parcellations remain scarce[23].

Recently, the group-level functional parcellation maps[19], characterizing a finer feature based on functional magnetic resonance imaging (fMRI) compared to Yeo's large-scale network-level atlas have been established[26]. By subdividing higher-order association cortical network into subcomponents, Wang et al.[21] demonstrated the association among refined subcomponents with multidimensional cognitive processes and health conditions. Using high-resolution images and group-level priori parcellation features, Kong et al.[20,27] developed individualized brain atlases in areal-level, exhibiting better behavioral prediction performance. Individualized areal-level brain parcellation also shows significant advantages in navigated neuromodulation and personalized treatment of neuropsychiatric diseases[23]. In addition, the areal-level functional parcellations of the infant cerebral cortex was established with meaningful cortical functional correspondence[28,29]. Notably, there are common 'border' and 'ectopic' variants across individuals, differing in their location, network associations, properties of subgroups of individuals, activations during tasks, and prediction of behavioral

phenotypes[4]. Thus, there are noteworthy challenges, especially functional homology, to capture the dynamic developmental process of areal-level parcellations for intersubject correspondence in functional organization. Moreover, a normative model of brain functional development based on individualized, areal-level homologous parcellation maps will facilitate a more precise characterization of developmental trajectories of the brain.

Here, we present the fine-grained areal-level individualized homologous functional parcellations (IHFPs) from childhood to adolescence (total age range: 8–21, total $N = 591$) (Fig. 1a). Subsequently, we delineated the normative growth curves of resting-state functional connectivity at areal-level (Fig. 1b). The patterns of the functional metrics suggested that the human brain undergoes continuous dynamic adaptation during development[8,11,15,16,29]. We then established the alignment between IHFPs and large-scale networks, to explore the additional insights revealed by fine-grained areal-level parcellations in network-level across adolescent development. We reveal that developmental trajectory in network-level exhibits differences from areal-level developmental trajectories, with higher variability between areal- and network-level trajectories in higher-order
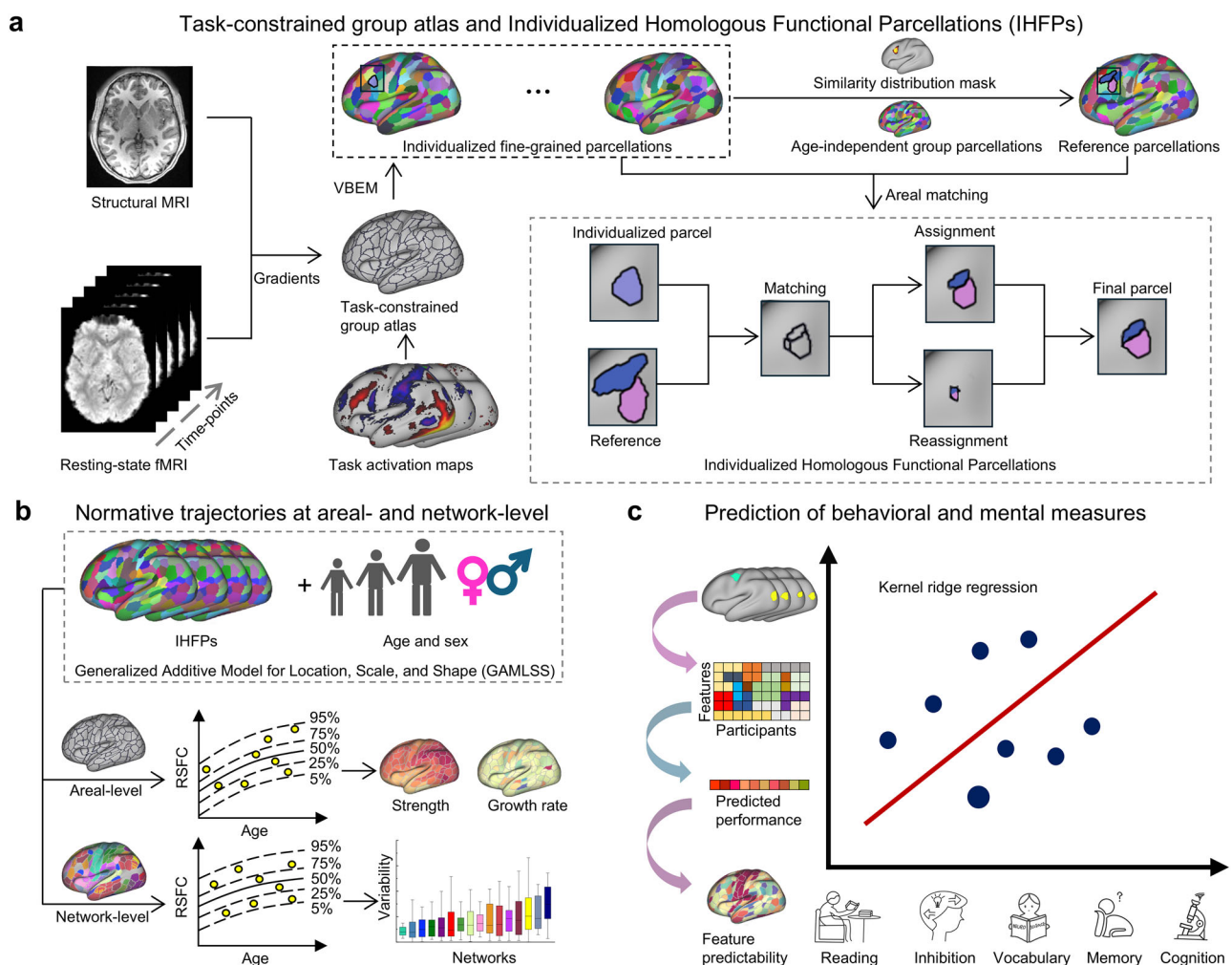

Fig. 1 | Study design overview and methodological approach. a We included structural and functional fMRI images from 591 typically developing subjects aged 8–21 years from the HCP-D dataset. First, task activation maps were integrated into the gradient-weighted Markov Random Field (gwMRF) model to constrain group-level parcellations. Then, individualized homologous functional parcellations (IHFPs) were constructed using a variational Bayes expectation-maximization (VBEM) algorithm[21,28], with areal matching procedures aligned to reference parcellations. For more details, please see Supplementary Fig. 2. b Resting-state functional connectivity can provide a criterion for characterizing functional development. Then, we leverage GAMLSS to calculate the developmental

trajectories of areal- and network-level functional connectivity and quantify the whole-brain distribution of its mean strength and growth rate. c We developed prediction models based on the within-system and between-system functional connectivity of IHFPs to predict adolescent cognitive behaviors. These models were compared to state-of-the-art individualized functional parcellations proposed by Kong et al. (noted as Kong2021)[21]. We selected 6 cognitive behaviors that stable and well-performed documented in previous studies[28,40,41], including reading, inhibition, vocabulary, working memory, fluid cognition, and crystallized cognition in predict models.

association networks. Finally, predictive modeling of cognitive behavior revealed that IHFPs outperform other individualized fine-scale atlas[20], indicating that functional homology alignment implement in our IHFPs framework enables more accurate mapping between brain function and behavior (Fig. 1c). Collectively, the insights and data suggest that fine-grained areal-level homologous parcellation enables better functional correspondence across individuals and that developmental trajectories derived from these functionally aligned regions provide valuable insights into the fine-scale maturation of human brain function.

Results

We utilized 591 high-resolution adolescent fMRI images, from the Lifespan Human Connectome Project in Development (HCP-D) study to construct IHFPs, spanning from childhood to adolescence, more demographic details, please see Table 1 and Supplementary Fig. 1. Specifically, we followed the standard HCP data processing pipeline[30], and extracted surface-based preprocessed blood oxygenation level-dependent (BOLD) signals in fs_LR_32k space. Then, we incorporated functional surface alignment boundary maps, task activation maps and resting-state functional connectivity (RSFC) to construct group-level, age-related parcellations as precise prior information for establishing an individualized atlas. To generate functional homologous brain areas across individuals, we performed homologous functional matching across all fine-grained individual brain parcellations to age-independent group-level parcellations to obtain the

IHFPs (Supplementary Fig. 2). To investigate age-related nonlinear growth patterns of functional representation using IHFPs, we applied the generalized additive models for local, scale, and shape (GAMLSS) to elucidate developmental trajectories in youth, with sex and in-scanner head motion as fixed effects and scanner sites as random effects[15,31–34]. Furthermore, we established the correspondence between homologous parcellations and large-scale networks, offering insights into the developmental patterns and interrelationships of brain function across fine-grained parcels within corresponding networks (Supplementary Fig. 3). Finally, we predicted cognition behaviors for application of our areal-level IHFPs.

Task-constrained group-level parcellations exhibit finer boundaries and inducing higher functional homogeneity

We first divided subjects from 8 years to 21 years into 5 distinct age groups for cross-sectional analyses that target specific age groups[12,14,15,28,35] (Table 1). The changes in the age-related and age-independent group-average gradient maps during development were relatively stable, with higher functional gradients predominantly observed in the middle frontal gyrus, supramarginal gyrus, precuneus, indicating stronger intersubject similarity in gradient boundaries within these regions (Fig. 2a, Supplementary Fig. 4a). As the number of iterations increased in the iterative surface alignment model (for more details please see the Methods), the variability in the functional gradient maps decreased significantly (Supplementary Fig. 4b, top panel). Age-independent local gradient maps began to stabilize around 7th iteration, and after 15th iterations, the variability became nonsignificant ($P = 0.12$, two-tailed paired-sample t-test between two consecutive iterations). Compared to the maps from the 1st iteration, the stabilized boundary map after 15th iterations revealed new gradient boundaries in the superior frontal gyrus and parietal cortex, indicating that the alignment process can uncover additional gradient information (Supplementary Fig. 4b, bottom panel).

The stabilized gradient boundary map was integrated into the gradient-weighted Markov Random Field (gwMRF) model[19], generating age-related group-level parcellations. To enhance boundary accuracy, we incorporated a task activation term into the MRF objective function, in addition to the original local gradient term, global similarity term and spatial connectedness term. Age-related and age-independent group parcellations were shown in

Table 1 | Demographic information of the HCP-D dataset

Age group	Age range (Mean ± SD)	Sex (M/F)	Subject number	fMRI scans number
Age group1	8–9 (9.08 ± 0.53)	27/58	85	339
Age group2	10–12 (11.35 ± 0.88)	61/61	122	482
Age group3	13–15 (14.37 ± 0.84)	80/84	164	656
Age group4	16–18 (17.29 ± 0.90)	48/57	105	418
Age group5	19–21 (20.52 ± 0.90)	54/61	115	456
Cognition behavior	8–19 (12.60 ± 2.66)	219/181	400	1591

Fig. 2 | The local gradient maps and group-level parcellations of HCP-D dataset. a Age-related local gradient maps computed by averaging individual local gradient maps after co-registering, as described in Wang et al.[29]. Only the left hemisphere is shown for visualization purposes; parcellations in right hemisphere are also identified, as shown in Supplementary Fig. 4a. **b** Age-related fine-grained parcellations were derived from local gradient maps, task-fMRI and RSFC patterns using the gwMRF (right hemisphere are shown in Supplementary Fig. 4c). **c** Mean intersubject variability of functional connectivity based on age-related and age-independent group-level parcellations was averaged within each age group, corrected by regressing out the mean intrasubject variability. Right hemisphere's intersubject functional connectivity variability is shown in Supplementary Fig. 4d. **d** Task-related inhomogeneity, measured by the standard deviation of task fMRI activation within each parcel, was compared between gwMRF and our task-constrained gwMRF age-related parcellations[20]. Lower task-related inhomogeneity indicates higher functional homogeneity. Distribution of data points was represented as each individual's task-related inhomogeneity. Statistical significance assessed using a two-tailed paired t-test, *$P < 0.001$. y, year.

a Age-related local gradient maps
8-9y, 10-12y, 13-15y, 16-18y, 19-21y, Age-independent

b Age-related fine-grained parcellations
8-9y, 10-12y, 13-15y, 16-18y, 19-21y, Age-independent

c Intersubject variability of connectivity
8-9y, 10-12y, 13-15y, 16-18y, 19-21y, Age-independent

d Task-related inhomogeneity of group atlas
Lower = Better
gwMRF
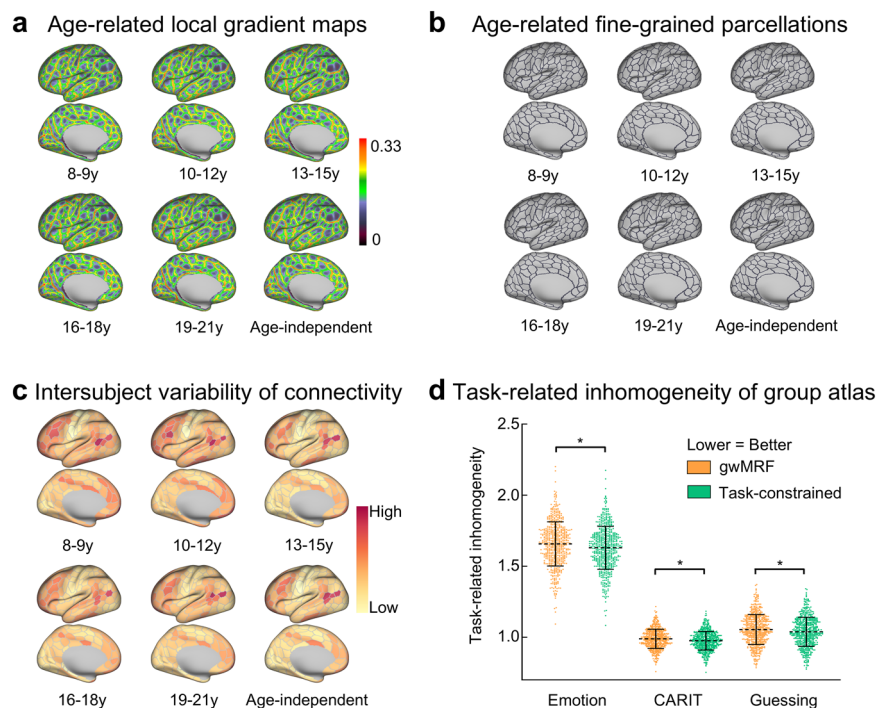Task-constrained
Emotion, CARIT, Guessing

Fig. 2b and Supplementary Fig. 4c. The primary motor cortex, occipital, and posterior cingulate cortex exhibited stable parcel topologies, whereas areas such as the lateral prefrontal cortex and posterior superior temporal gyrus showed high variability of parcel topologies across age-related group-level parcellations. We observed that the boundaries formed by the combination of large-scale network boundaries and corresponding regional parcellations generally aligned, such as the boundary of the posterior cingulate cortex parcellation is similar to that of the default A in the Yeo 17-networks parcellation[26]. This alignment provides valuable guidance for the subsequent matching of areal-level parcellations with large-scale networks. The intersubject variability[36] in functional connectivity within each age group was highest in the prefrontal and posterior superior temporal regions and exhibited an age-related decrease in the middle frontal gyrus, inferior parietal lobule, and superior temporal gyrus (Fig. 2c and Supplementary Fig. 4d).

Subsequently, we compared the functional inhomogeneity between the original gwMRF[19] and our task-constrained gwMRF model using three HCP-D task-fMRI datasets ($N = 587$ for *Emotion*; $N = 577$ for *Conditioned Approach Response Inhibition Task* (*CARIT*); $N = 588$ for *GUESSING*)[37]. For each subject, functional inhomogeneity was averaged across all parcels and compared within each cognitive domain[19]. The group-level parcellations constrained by fMRI task activation exhibited significantly lower functional inhomogeneity within each of the three tasks (Fig. 2d, all *P*-values < 0.001, two-tailed paired *t*-test), enabling the generation of high-quality individual parcellations for developmental studies.

Mapping normative trajectories of the areal-level functional connectivity in youth

We employed task-constrained, age-specific group-level parcellations as priors, rather than age-independent group-level parcellation, in order to preserve the unique topological features characteristic of each age group as much as possible. Applying the contiguous multi-session hierarchical Bayesian model (cMS-HBM)[20], we generated individualized parcellations at finer-scales for each age group. The cMS-HBM method was selected because it provides stable mapping results and consistent region labeling, even in the presence of high individual variability and poor data quality[20]. However, cross-individual alignment of functional parcellations based on group priors does not guarantee functional homology between parcels[24]. To address this, we applied a functional homologous alignment approach across individual parcellations to obtained IHFPs (for more details please see the Methods). Examples of functional homologous parcellations for representative participants across age groups are shown in Fig. 3a and Supplementary Fig. 5a. The group-level parcellation comprised 398 cortical parcels, and all individuals retained at least 396 parcels. The occasional absence of one or two parcels per individual likely reflects inherent functional variability. For developmental trajectory analyses, each parcel retained data from at least 92% of participants, ensuring a balance between capturing individual functional variability and maintaining result reliability. We then performed split-half reliability analysis to assess the reliability of the parcellations[3]. The reliability of parcellations was evaluated both within intersubject and intrasubject, quantifying the stability of IHFPs using the distribution of Dice's coefficients and normalized mutual information (NMI). The mean of Dice's coeffcent for each parcel across cerebral cortex was calculated by averaging across pairs of subjects, both intrasubjects and intersubjects. The mean Dice's coefficient for intrasubject comparisons was 77.5%, significantly higher than the 66.6% for intersubject comparisons ($P < 0.001$, two-tailed two-sample *t*-test, Fig. 3b and Supplementary Fig. 5b). We also plotted the NMI distribution for intrasubject and intersubject test-retest reliability (Fig. 3b). The mean intersubject NMI was 0.90, while the mean intrasubject NMI was 0.93, further comfirming stability of IHFPs ($P < 0.001$, unequal variance assumed, one-tailed).

To more accurately capture patterns of brain functional development, we used a GAMLSS model to fit nonlinear developmental trajectories of RSFC based on IHFPs, including global mean, within-system and between-system functional connectivity (Fig. 3c, Supplementary Figs. 5c and 6–7).

The strength of normative trajectory for both global mean and between-system functional connectivity exhibited similar spatial patterns, peaking in the somatosensory cortex and visual areas at each year. Growth rates were negative from ages 8 to 10 in the primary motor cortex, superior temporal sulcus, inferior temporal sulcus, and inferior frontal gyrus, gradually approaching zero thereafter for global mean functional connectivity. However, the growth rate continued to increase up to age 21. In prefrontal cortex, the growth rates were increased into positive by age 20. For within-system functional connectivity, the highest functional connectivity were observed in the somatosensory and parietal cortices, exhibiting a decreasing trend with age. The corresponding growth rates also transitioned from negative values toward zero over time. In the prefrontal cortex and lateral occipital sulcus, the growth rates were positive between ages 8 and 10, gradually declining to zero thereafter. By age 19, growth rates in the primary motor and visual cortices shifted to positive values but began to decrease again, turning negative by age 21.

To assess the potential influence of age group sample size imbalance on the results, we created balanced dataset by matching sample size, scanner sites, and head motion (Supplementary Table 1). We modeled areal-level developmental trajectories of global mean, within-system, and between-system functional connectivity using the balanced dataset (Supplementary Fig. 8). The strength of the normative trajectory at each year in the balanced dataset closely mirrored that observed in the discovery cohort. The consistency of growth rates between the balanced and discovery cohorts highlights the robustness of the results. For both the global mean and between-system functional connectivity, the growth rate within the primary motor cortex also exhibited negative growth which similar to the discovery cohort. Furthermore, for within-system functional connectivity, the number of regions showing positive growth rates in the prefrontal cortex was reduced as age increased. Despite these discrepancies, the overarching developmental patterns were preserved. These results suggest that although differences in sample size introduced some fluctuations in the developmental trajectories, the overall patterns observed in the control group closely mirrored those of the discovery cohort.

Higher variability of developmental patterns exhibits in higher-order association cortices

To investigate the hetergeneity of developmental patterns across the cerebral cortex, we established correspondences between our areal-level IHFPs and large-scale networks (for more details please see the Methods). Specifically, we first assigned each parcels of IHFPs into a canonical 17-network parcellations[26], and then averaged these individualized networks to obtain the network probability map. Further, we thresholded the probability map of each network to construct an alternate functional 17-networks parcellation (Fig. 4a), with striped parcellations indicate that a parcel corresponding to multiple networks in the assignment, while gray regions denote parcels where the stability of network matching falls bellow the set threshold (Fig. 4a shows the 92% threshold, with results from 98% to 86% in 2% decrements in Supplementary Fig. 9). Age-independent parcel-to-network matching showed predominantly one-to-one relationships in sensorimotor, auditory, and visual networks. In contrast, alternate parcellations were more frequently in higher-order association cortices. The limbic network, located around the medial wall, often exhibiting lower signal-to-noise ratio (SNR), was excluded from further analysis[38].

Based on the parcel-to-network matching procedure, we calculated the parcel-weighted functional features within each matched network and used the GAMLSS model to fit their normative trajectories (Fig. 4b). To examine the normative trajectories constructed using the alternate functional 17-network parcellation derived from IHFPs, we also conducted comparative analyses using the traditional group-level Yeo 17-network parcellation. Developmental trajectories of global mean functional connectivity across all networks generally exhibited a downward trend. In terms of developmental rates, the temporal-parietal, default B, ventral attention B, and control networks exhibited a positive growth trend with age. By contrast, the default A, somatomotor, and visual networks showed growth rates that increased
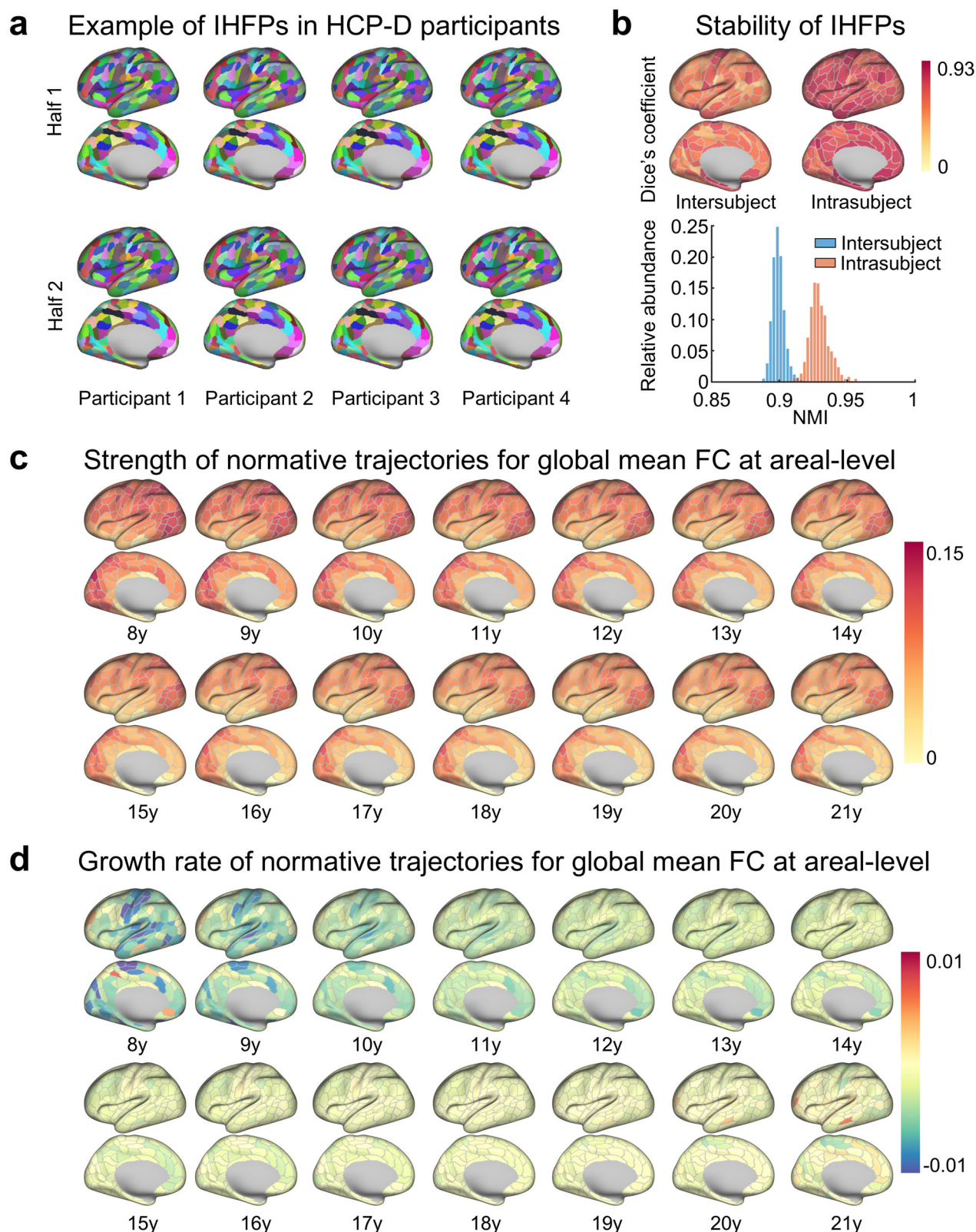
Fig. 3 | Strength and growth rate of developmental trajectories in youth based on IHFPs at areal-level. a Example of areal-level parcellations constructed using the IHFP technique. Resting-state fMRI timeseries were split in half, with parcellations generated from each half of the timeseries. **b** Stability of IHFPs was assessed using the Dice's coefficient and NMI across intrasubject and intersubject homologous parcels. **c** Strength of normative trajectories of global mean functional connectivity was quantified as the 50th percentile at each age and visualized on the cortex using the age-independent group-average parcellation. **d** Growth rate of normative trajectories of global mean functional connectivity was quantified as the first derivative of the 50th percentile at each age and visualized on the cerebral cortex using the age-independent group-average parcellation. Only left hemisphere is shown here; right hemisphere is displayed in Supplementary Fig. 5. NMI, normalized mutual information; y year.
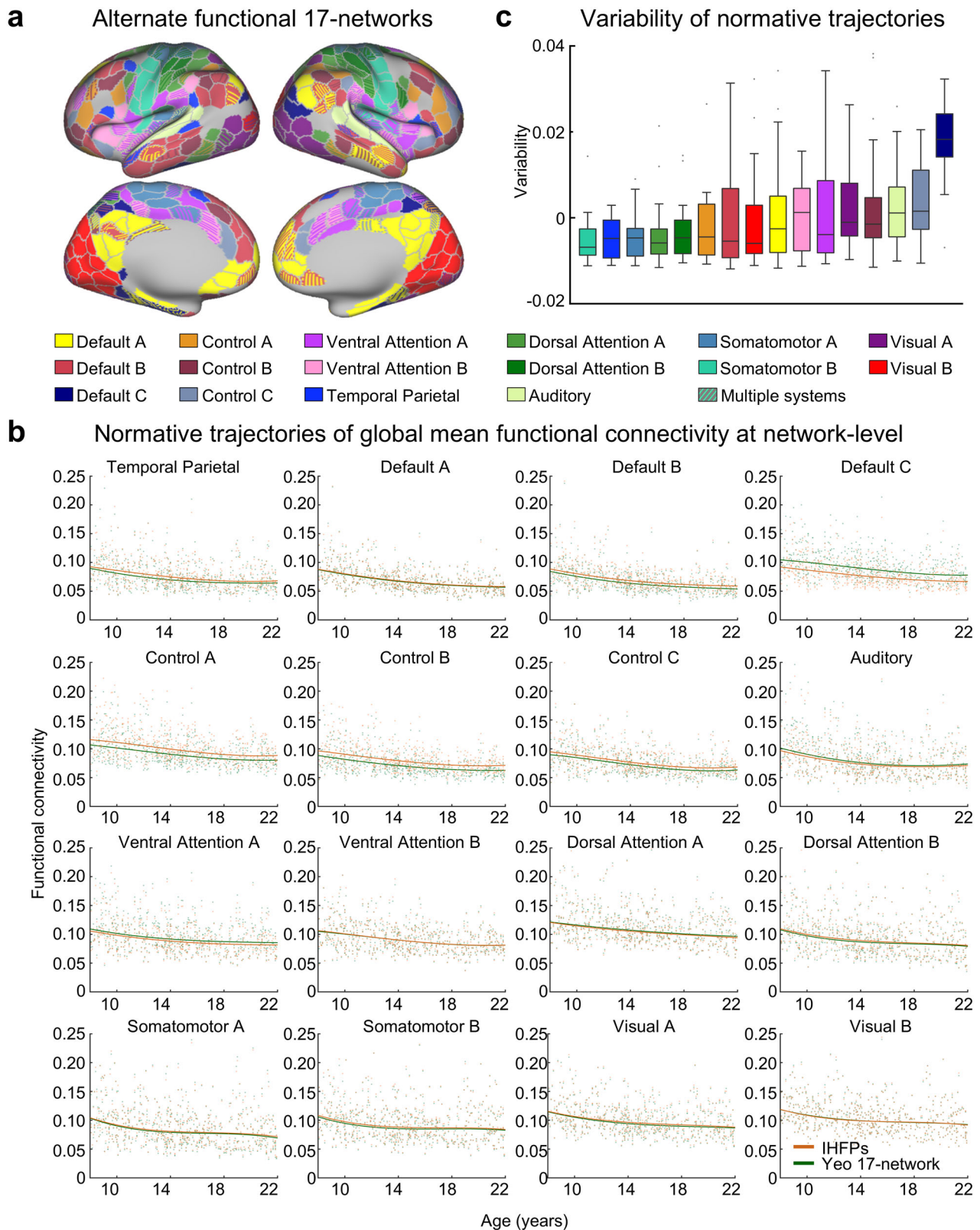
Fig. 4 | Fine-grained areal-level IHFPs assigned to canonical 17-networks.
a Alternate functional 17-networks parcellation calculated by averaging the network-assigned IHFPs (with threshold from 98% to 86% in 2% decrements in Supplementary Fig. 3). Striped colors indicate parcels that are assigned to multiple networks during the assignment procedure. **b** Normative trajectories of global mean functional connectivity for each assigned network based on IHFPs and Yeo 17-network parcellations. These results indicate that the system-level normative model trajectories exhibit high reproducibility in IHFPs compared with group averaged large-scale network parcellations. **c** Variability of normative trajectories of global mean functional connectivity, represented by the mean absolute deviation of each parcel's global mean functional connectivity related to its corresponding functional network, regressed out the number of parcels assigned to each network. Compared to group averaged large-scale network parcellations, the normative model trajectories based on IHFPs exhibit spatial heterogeneity at the system level. Data points for constructing box plots were calculated as variability for each parcel's trajectory corresponding to network-level trajectory.
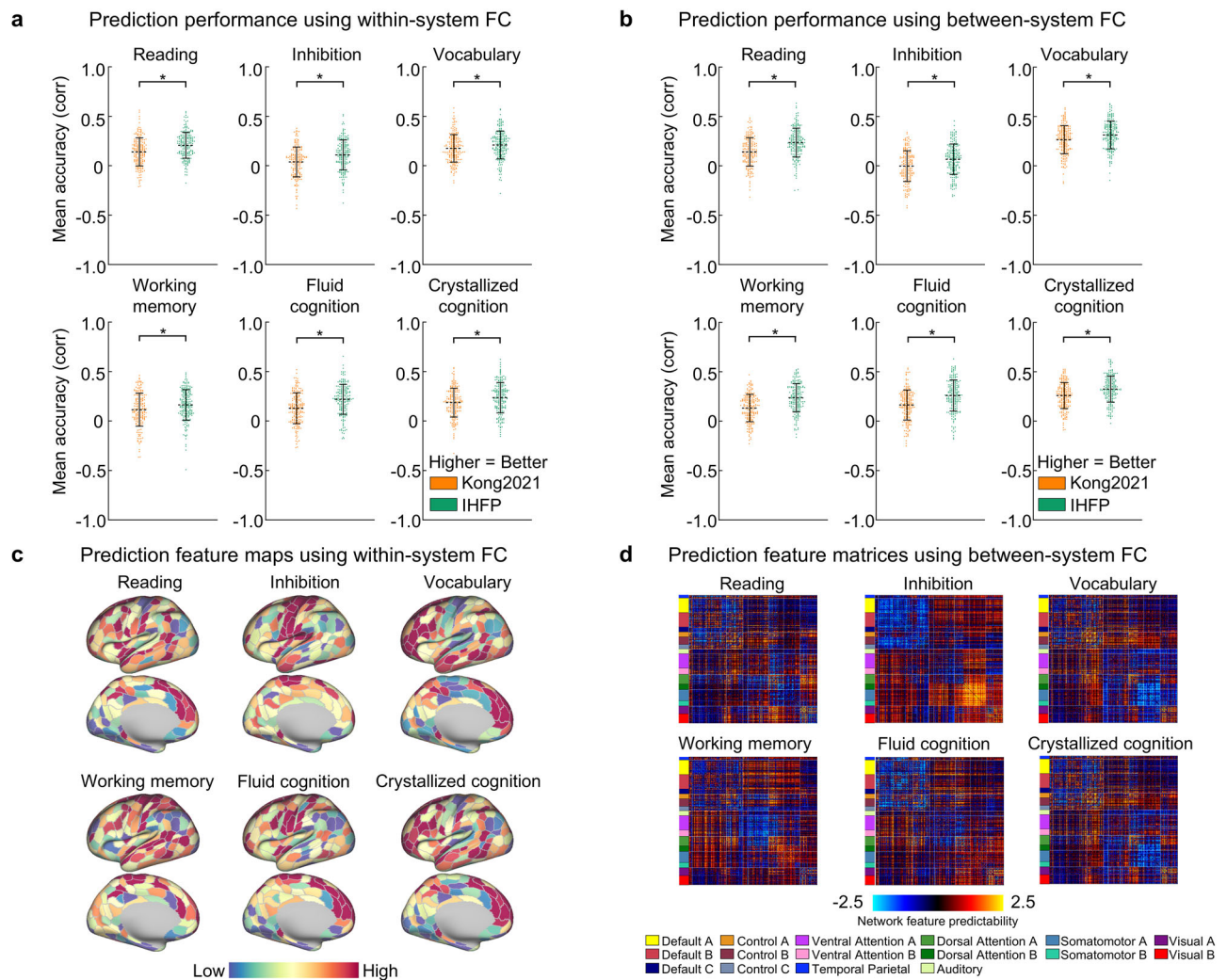
Fig. 5 | Prediction performance and features for behavioral measures using kernel ridge regression. a Prediction performance using within-system functional connectivity based on the Kong2021 atlas[21] and our IHFPs. The behavioral measures include reading, inhibition, vocabulary, working memory, fluid cognition, and crystallized cognition. **b** Prediction performance using between-system functional connectivity based on Kong2021 atlas and our IHFPs. Distribution of data points was calculated through 20 random replications of 10-fold nested cross-validation, resulting in 200 predictions. **c** Predictive-feature metrics for each behavioral measure using within-system functional connectivity, with gray lines depicting parcellation boundaries. Right hemisphere is displayed in Supplementary Fig. 11. **d** Prediction feature maps when using between-system functional connectivity to predict behavioral measures, with white lines depicting network boundaries. For visualization, the values within each matrix of feature predictability were divided by their standard deviations (across all entries in the matrix). *$P < 0.0001$, two-tailed paired t-test.

initially but declined at later ages (Supplementary Fig. 10). Results based on the alternate functional 17-network parcellation derived from IHFPs closely resembled those from the Yeo 17-network parcellation, indicating that IHFPs effectively recapitulate network-level developmental patterns.

To investigate the variability of normative trajectories of fine-grained areal-level global mean functional connectivity within each large-scale networks, we then calculated the mean absolute deviation between each parcel's trajectory and its corresponding network-level normative trajectory, regressed out the number of parcels assigned to each network. The variability of normative trajectories within each network was quantified by averaging the mean absolute deviation for all parcels within the network. The variability of normative trajectories across large-scale networks generally shifted from primary and unimodal sensory and motor cortices to higher-order association cortices (Fig. 4c). Specifically, the default mode, control, and ventral attention networks exhibited higher variability of normative trajectories than the temporoparietal, and sensorimotor networks. These results demonstrate that the normative trajectories of IHFPs exhibit heterogeneous variability across cortical

hierarchies, suggesting that IHFPs can provide precise insight into adolescent developmental patterns.

Higher performance in predicting behavior with functional connectome properties based on IHFPs

Having established the normative trajectories in youth, we further used kernel ridge regression to predict behavioral outcomes based on functional connectome properties from IHFPs, comparing the results with another fine-grained individualized parcellation method proposed by Kong et al. (noted as Kong2021)[20]. We selected 6 cognitive behavioral measures from 400 individuals in HCP-D dataset, which are a subset of the behavioral measures analyzed in previous studies[27,39–41]. Within-system and between-system functional connectivity were calculated using both IHFPs and Kong2021 atlases as neuroimaging features for prediction. A nested cross-validation procedure, with 20 random replications of 10-fold nested cross-validation, was employed to evaluate the predictive models. Figure 5a, b shows the prediction accuracies for the six behavioral measures using the two different parcellation approaches. For all behavioral measures, the

prediction performance using within-system functional connectivity based on IHFPs was significantly higher than that based on Kong2021 (Fig. 5a, all $P < 0.0001$, two-tailed paired t-test) after correction for multiple comparisons (FDR $q < 0.05$), with the mean prediction accuracy for fluid cognition in IHFPs reaching highest level (mean accuracy = 0.21 ± 0.15). Similarly, prediction using between-system functional connectivity with IHFPs outperformed Kong2021-based predictions (Fig. 5b, all $P < 0.0001$, two-tailed paired t-test with FDR corrected), with notable predictive performance for fluid cognition in IHFPs (mean accuracy = 0.25 ± 0.15).

We further explored the topography of predictive network features for each behavioral measure. We applied Haufe transformation to invert all prediction models into forward models, which allowed us to obtain predictive feature matrices[39]. Haufe's inversion approach generated positive (or negative) predictive feature maps representing the weight maps of the predictive models. Using within-system functional connectivity for behavioral predictions enabled a more detailed topological analysis of contributions from different brain regions to specific behavior predictions (Fig. 5c). For behavioral predictions, between-system functional connectivity feature matrices were partitioned into blocks according to network structures (Fig. 5d). We also computed within-system and between-system functional connectivity predictive feature matrices for the Kong2021 atlas, which revealed a similar whole-brain spatial distribution pattern to that predicted by IHFPs (Supplementary Figs. 12–13).

In predicting behavior of reading, the within-system functional connectivity features in the dorsal attention, ventral attention, and control A networks displayed positive predictivity, while in the default mode and visual networks showed negative predictivity. When using between-system functional connectivity as a feature for reading behavior prediction, functional connectivity between the visual, dorsal attention, ventral attention, and control networks showed higher positive predictivity, followed by the sensorimotor, temporal parietal networks. However, between-system functional connectivity in the default C and the other two default mode sub-networks (default A and B) exhibited negative predictivity. These results suggest that reading behavior is closely associated with communication among the visual, dorsal attention, and ventral attention networks, as well as the involvement of sensorimotor and control networks.

In predicting behavior of inhibition, the within-system functional connectivity in the sensorimotor and auditory networks demonstrated strong positive predictivity, while the default mode and control networks exhibited negative predictivity. Additionally, within-system functional connectivity in the default B/C, control, and ventral attention networks showed negative predictivity. For the between-system, the functional connectivity between sensorimotor and visual networks exhibited significantly higher predictive performance compared to other networks. These findings suggest that inhibition behavior is more closely related to the primary visual and sensorimotor networks and inversely related to higher-order association cortices.

In predicting behavior of vocabulary, the within-system functional connectivity showed positive predictivity which was observed in the default B/C and control networks, while negative predictivity was found in the somatomotor and default A networks. As for between-system functional connectivity, the functional connectivity between the control, ventral attention, dorsal attention, and somatomotor B networks showed strong positive predictivity. These results suggest that vocabulary behavior is primarily associated with the default mode, control, ventral attention, and dorsal attention networks.

Working memory behavior is assessed using a sequencing test that requires immediate recall and ordering of visually and aurally presented stimuli[42]. For the within-system functional connectivity, we found that the sensorimotor network showed high positive predictivity, while the default mode network showed high negative predictivity. When using between-system functional connectivity for predicting working memory behavior, functional connectivity between the visual and most other networks (except default A/B) showed positively predictive. Furthermore, the between-system functional connectivity in default mode and control networks with

the auditory, ventral attention, dorsal attention, and sensorimotor networks also showed strong positive predictivity. In total, working memory behavior, compared to other behaviors, involves a broader range of whole-brain functional networks, including visual, sensorimotor, control, and default mode networks, reflecting extensive inter-network communications.

For fluid cognition, the within-system functional connectivity showed positive predictivity in the somatomotor B and default B networks, while the somatomotor A, visual B, and default A networks showed negative predictivity. When using between-system functional connectivity for predictions, the sensorimotor and visual networks exhibited strong positive predictivity. Additionally, positive predictivity was observed in functional connectivity between the ventral attention and default mode networks. In contrast, intra-network functional connectivity within the control and default mode networks was mostly non-significant.

Crystallized cognition provides a more comprehensive assessment of individual and group verbal reasoning abilities, relying on accumulated learning experiences and remaining relatively stable throughout adulthood. The predictive-feature matrix of crystallized cognition was similar to that for vocabulary behavior, both reflecting feedback on past learning. The within-system functional connectivity features in the default B/C and control networks showed high positive predictivity, while negative predictivity was observed in the somatomotor and default A networks. For between-system functional connectivity, intra-network connectivity within the auditory and control networks exhibited strong positive predictive value, followed by inter-network connections linking the control, ventral attention, dorsal attention, and somatomotor B networks. In contrast, intra-network connectivity within the dorsal attention B, somatomotor B, and visual A networks demonstrated marked negative predictive value.

Discussion

Establishing a proper functional correspondence between individuals is a prerequisite for mapping a normative trajectory of adolescent development. This study explored the potential of refined maps with homology to establish a normative trajectory of adolescent development. Based on refined individual-level brain functional parcellation technology, we are able to identify homologous functional regions across individuals (IHFPs). Normative trajectories of global mean functional connectivity demonstrated spatial heterogeneity, with the strongest values consistently localized to the somatosensory, parietal and visual cortices across all developmental stages. The peak of functional connectivity developmental trajectories occurs during late childhood (ages 8–9), suggesting that as children transition into adolescence, the brain undergoes connectivity pruning, information exchange across brain networks becomes more distributed. Then, we found that in the process of assigning refined areal-level parcellations to large-scale networks, parcels in higher-order association cortices are more unstable, showing that one parcel may belong to several potential networks. Moreover, areal-level homogeneous developmental trajectories show heterogeneous distribution patterns of variability in large-scale networks across cerebral cortex, with higher variability of developmental patterns exhibits in higher-order association cortices. This pronounced variability observed in the developmental trajectories of these higher-order association cortical regions during adolescence may reflect the fact that adolescence is a critical period for large-scale reorganization of functional architecture and information processing in the brain. Importantly, the IHFPs capture the idiosyncrasies of the subjects, with functional connectivity based on IHFPs can better predict individual behavioral measures than the current most widely used individualized parcellation approach[20]. In total, these findings suggest that establishing fine-grained areal-level brain functional parcellations with homology between individuals is important in constructing normative trajectories during development and has potential value in delineating the linking between individual imaging phenotypes and behavioral measures.

Previous studies based on group-level brain parcellations have mapped standardized developmental trajectories and identified brain functional connectivity patterns during childhood development[13,16,43,44]. Currently, widely adopted group-level brain atlases include large-scale and

fine-grained areal-level functional parcellations based on functional homogeneity[19,26], anatomical atlases derived from morphological features[45–47], and fusion parcellations constructed using multimodal brain imaging data[17]. These group-level atlases can be readily applied to individual neuroimaging datasets for connectomic analyses, forming a standardized pipeline commonly used in contemporary neuroimaging research. However, group-level parcellations can obscure interindividual variability in brain structure and function, failing to capture the unique patterns of each individual[48–51]. These variations were found to be most prominent in frontoparietal networks[14] and involved differences in parcel size, location, and functional connectivity[24]. Therefore, constructing individualized brain functional parcellations is beneficial for emphasizing individual specificity, as the topological features of an individual's brain function are better suited for predicting behavior and show a genetic basis[52]. Recently, Sun et al.[15] developed large-scale individualized brain functional atlases and mapped standardized functional connectivity trajectories across the human lifespan. These results revealed the unique developmental characteristics of brain functional connectome during childhood. However, large-scale networks fail to capture the fine-grained topological features within networks. Sydnor et al.[35] based on fine-grained group-level brain parcellations, mapping the intrinsic fMRI BOLD fluctuation amplitudes during childhood and adolescence and demonstrated developmental functional variability along the sensorimotor-association axis. These BOLD fluctuation amplitudes were quantified using group-level surface atlases, which are based on a strong assumption that group-level parcellations preserve homologous correspondence across individuals. However, Li et al.[24] proposed a homologous functional regions mapping approach and showed that individualized homologous regions exhibited significant intersubject variability, and RSFC among these regions was more predictive of fluid intelligence than group-level brain parcellations. Thus, a central challenge in constructing individualized, fine-grained areal-level functional brain parcellations lies in establishing inter-individual correspondence across homologous brain regions. Although previous studies have advanced parcellation granularity at the individual level[20], significant gaps remain in methods for ensuring functional homology across individuals. Relying solely on spatial overlap as a criterion for homology is insufficient[24], as it can result in the omission of spatially variable but functionally critical regions, which may underlie critical individual-specific features. In this study, we propose a novel approach —Individualized Homologous Functional Parcellation (IHFP)—which incorporates both spatial overlap and temporal correlation to identify homologous regions across individuals. Our method preserves over 99% of the cortical regions at the individual level while ensuring inter-subject functional correspondence. Functional connectivity profiles derived from IHFP demonstrated better performance in predicting individual behavioral measures compared to the widely adopted Kong2021 individualized parcellation approach[20]. It is important to note that, although our method enables the establishment of areal-level inter-individual functional homology, the concept of functional homology in neuroscience remains inherently complex and multidimensional, and currently lacks a universally accepted definition. Future research should aim to further clarify the fundamental nature of functional homology and explore methodological innovations to better capture its underlying principles.

After constructed IHFPs, we mapped developmental trajectories based on the fine-grained areal-level brain functional homologous regions across subjects, allowing for analyses at the appropriate level of granularity. We found that the normative trajectories of global mean and between-system functional connectivity strengths reveal similar spatial patterns, characterized by the highest connectivity in the somatosensory and visual cortices, which gradually declines with age. Compared to unimodal cortices, the global mean and between-system functional connectivity strengths in the transmodal association cortices exhibit greater spatial variability, while similarly showing a decreasing trend with age. These results suggest that higher-order association cortices exhibit increased variability compared to other unimodal systems, which consistent with previous studies[15,35]. In the within-system functional connectivity, we found the highest connectivity

was observed in the somatosensory and parietal cortices, exhibiting a decreasing trend with age. The corresponding developmental rates also shifted from negative values toward zero over time. The spatial differences in the normative trajectories of within- and between-system functional connectivity suggest that system segregation during adolescence may follow spatially heterogeneous trajectories[15]. Future studies leveraging graph-theoretical analyses of homologous developmental trajectories in functional connectivity will help to elucidate the maturation of system-level brain network architecture during adolescence and its association with social, physical, and mental health outcomes in adolescence and adulthood[8]. Overall, the fine-grained normative trajectory presented here offers an important reference for studying the typical functional development of the human brain in youth.

The process of areal-level parcel matching large-scale networks showed that some parcels in higher-order association cortices corresponded to multiple different networks, which have been previously shown to exhibit high variability in network assignment[24,53,54]. Specifically, we observed the greatest variation in network assignment within the default mode network, specifically in the overlap between default A and default B networks. Using individualized precise fMRI imaging techniques, Braga et al.[22] demonstrated that the default network consists of two separate networks with adjacent regions, one of which is coupled to the hippocampal formation. Our results show that these subnetworks of the default network are detectable at the individual level and exhibit significant interindividual variability, with overlapping sub-network regions across subjects. Previous study has demonstrated that these correspondence of functional boundaries across different brain parcellation schemes is highest in visual and motor networks, but notably lower in the default mode, central executive, and salience networks[55]. This pattern reflects two main factors: variability across parcellation methods and the spatial heterogeneity of functional boundary stability across the cortex. This induced boundary definitions are particularly unstable in association cortices[53]. Our findings extend this observation to adolescence—a period of profound brain maturation—demonstrating that such boundary instability persists throughout this stage. Adolescent brain development is marked by a transition from locally organized processing to more distributed and functionally integrated network configurations, particularly within association cortices[56]. These regions engage more flexibly across network communities, introducing uncertainty in model-based assignments and likely reflecting cortical boundaries that have yet to fully consolidate[57]. This likely contributes to the instability of network affiliation within association cortices during adolescence. Furthermore, we found that the normative trajectories at the network level displayed a marked reduction in global mean functional connectivity with age in default and control networks. In contrast, the somatomotor and visual networks showed more stable and conservative changes throughout development. By quantifying the variability of the normative trajectories for homologous parcels within each network, we found that higher-order association networks exhibited more variability compared to unimodal networks. These findings are consistent with previous studies that demonstrate spatio-temporal variability in regional developmental trajectories is organized along a hierarchical distribution, with higher-order association cortices showing the greatest variability[35].

Individual brain functional connectivity exhibited better performance for tracking individual behavioral variability than anatomical or diffusion MRI-based connectivity[39,58–60]. Furthermore, connectivity within functional brain networks has also been linked to multiple dimensions of psychopathology, suggesting the potential for developing connectivity-based biomarkers in psychiatry[61]. Using the MS-HBM technique, Kong et al.[20] constructed individual-specific cortical parcellations and revealed that RSFC derived from these MS-HBM parcellations achieved superior behavioral prediction performance compared to group-level brain parcellations. These individual-specific hard parcellations also performed better when compared with the principal gradients detected by reducing the dimensionality of RSFC to obtain the main functional organization patterns[40]. We selected 6 cognitive behavioral measures, which are central to adolescent

cognitive development and support functions such as emotion regulation and intellectual engagement[62–66]. We demonstrated that within-system and between-system functional connectivity derived from IHFPs outperforms the performance derived from Kong et al.[20] parcellations in predicting behavioral measures. Functional connectivity-based predictive feature metrics revealed that distinct brain network features support the prediction of different cognitive functions. Recently, Chen and colleagues[39] established shared and unique brain network features predicting different dimensions of individual behaviors. Our results extended this study, demonstrating predictive features derived from within-system functional connectivity were significant differences in the distribution patterns across the cerebral cortex for different cognitive functions. These findings underscore the importance of studying the relationships between brain functional organization and multidimensional behavior using fine-grained IHFPs.

Although this study benefited from a large sample and high-quality developmental data, several limitations should be noted. First, the current study used cross-sectional data, but previous study has shown that cross-sectional data can underestimate longitudinal trends[67]. However, there is still a lack of longitudinal brain imaging data spanning the entire adolescent developmental period. The Adolescent Brain Cognitive Development (ABCD) study is continuing to collect longitudinal data, offering a unique opportunity to explore neural development over time in young participants[68]. In the future, we can further establish developmental trajectory curves based on the ABCD longitudinal dataset. Second, the individualized homologous brain parcellation algorithm we developed is based on a group-level parcellation as prior, and the procedure for matching homologous functional regions across individuals may introduce bias. Functional homology has long been sought as the ideal solution by personalized brain maps. However, the variability in brain function makes perfect homology difficult to guarantee, and there is a lack of systematic experimental paradigms that can precisely capture brain activation patterns at the individual level to validate functional homology across individuals. Recently, Rajimehr et al.[69] used high-resolution fMRI data to parcellate the entire cerebral cortex into 24 functional networks based on individual responses to rich audiovisual movie stimuli. The topography of these networks was precisely characterized, with each network being assigned to a specific sensory or cognitive processing function. Thus, leveraging naturalistic stimuli to collect high-density fMRI data at the individual level may be used to create an individualized fine-grained areal-level brain functional atlases and enable more precise functional homology across parcels at the individual level. Third, the current study focused only on the cortical regions, overlooking the homological parcellation of subcortical structures. Cortico-subcortical circuits support communication functions and the integration of information within large-scale brain networks[70], and they exhibit dysfunction in neurodegenerative diseases[71,72]. Future work on fine-grained functional parcellation of individualized subcortical structures will significantly enhance our understanding of the maturation processes of subcortical structures during development.

Methods

Subjects and image acquisition
Subjects used in this study were collected by the Lifespan Human Connectome Project in Development (HCP-D) study. The HCP-D 2.0 release contained 1300+ healthy human participants, ages 5–21 years, acquired at four sites[73]. We included 591 typically developing children, adolescents, and young adults aged 8–21 years after applying inclusion criteria (excluding subjects with more than 50% frames that have framewise displacement (FD) > 0.2 mm, and within the age range of 5 to 7 years for varying duration of scan), as demonstrated in Table 1 for discovery dataset and Supplementary Fig. 1 for balanced dataset. All necessary ethical guidelines were adhered to throughout the data collection process.

Images were acquired across four sites using Siemens 3 T Prisma scanner with a standard 32-channel head coil. T1-weighted (T1w) images were acquired by multi-echo 3D magnetization prepared rapid gradient echo (MPRAGE) sequence: 0.8 mm isotropic voxels, TR (repetition time) /

TI (inversion time) = 2500/1000 ms, TE (echo time) = 1.8 / 3.6 / 5.4 / 7.2 ms for each scan site, FA (flip angle) = 8 deg, FOV (Field of View) = 256 × 240 × 166 mm³, matrix size = 320 × 300, 208 sagittal slices, in-plane (iPAT) acceleration factor of 2. T2-weighted (T2w) images were obtained with same spatial resolution using the variable-flip-angle turbo-spin-echo 3D SPACE sequence with TR / TE = 3200 / 564 ms; FOV and matrix size were the same as T1w.

Resting-state fMRI (rs-fMRI) data were acquired using T2-weighted scans sensitive to the BOLD signals contrast with a 2D multi-band gradient-recalled echo-planar imaging (EPI) sequence (TR / TE = 800 / 37 ms, FA = 52 deg) and 2.0 mm isotropic voxels covering the whole brain (72 oblique-axial slices). The acquisition parameters of task fMRI (tfMRI), including three tasks (GUESSING, CARIT, Emotion), were identical to rs-fMRI except the number of frames collected per run (rs-fMRI = 488; GUESSING = 280; CARIT = 300; Emotion = 178). More details about imaging protocols see Harms et al.[37]. All ethical regulations were followed during data analysis.

MRI processing
The HCP-D data had been processed with the HCP processing pipeline[30]. All T1w and T2w MR images were pre-processed under distortion correction, denoising, N4 bias correction, and MNI standard space registration[74]. The rs-fMRI data was processed including head motion correction, intensity normalization, bias field correction, ICA-FIX denoised and transformation to an isotropic 2-mm MNI atlas space[75], and registering into fs_LR_32k mesh to produce a Connectivity Informatics Technology Initiative (CIFTI) format with a BOLD time series for each functional run[39]. As previous studies reported that the ICA-FIX is not effective enough in removing global physiological noise and motion-related artifacts[76,77]. Additional processing steps were performed following the methodology outlined by Li et al.[78]. Firstly, FD of participants were estimated by fsl_motion_outliers. Then, volumes with FD > 0.2 mm were marked as high-motion frames. If the percentage of marked frames is above 50% percent, corresponding BOLD runs were further removed. Subsequently, linear regression was applied to account for multiple nuisance regressors, including six motion correction parameters and their temporal derivatives. Finally, each rs-fMRI scan was smoothed with a 6 mm full-width at half-maximum (FWHM) kernel.

Data analysis
Definition of age groups. We categorized participants into five age groups to ensure balanced distribution in terms of gender, sample size, and age range. These groups include late childhood (8–9 years), early adolescence (10–12 years), middle adolescence (13–15 years), late adolescence (16–18 years), and early adulthood (19–21 years). This stratification offers two key advantages. First, age-related parcellations are more appropriate for cross-sectional analyses that target specific age groups[12,14,15,28]. Second, reliable and stable age-specific parcellations require a sufficiently large dataset, ensuring robustness in subsequent analyses[79].

Task activation map. There are three distinct, but interrelated fMRI tasks of information processing domains in HCP-D datasets, including emotion processing, reward/loss anticipation and consumption, and inhibitory control processes. Task fMRI analysis was performed using an adaption of FSL's FEAT analysis pipeline[30,79,80], with task effects estimated through a generalized linear model (GLM). To the end, we obtained the individual and group task activation maps using a threshold ($|Z| > 5.01$)[73].

Selected behavioral measures. We selected six cognitive behavioral measures, a subset of the behavioral measures analyzed in previous studies[27,39–41], including reading, inhibition, vocabulary, working memory, fluid cognition and crystallized cognition. Fluid cognition refers to cognitive abilities without prior knowledge including inhibition and working memory, while crystallized cognition relies on accumulated experience including reading and vocabulary[81]. Both fluid and

crystallized cognition are important resources for cognitive development, such as effective emotion regulation and intellectual engagement[62–66]. Reading reflects adolescents' ability to recognize and pronounce letters and words, and together with vocabulary, serves as an index of reading experience[82,83]. Both are strongly associated with neural efficiency shaped by prior learning and remain relatively stable across the adult lifespan[66]. In contrast, working memory and inhibition are linked to reading speed and comprehension, and both reflect the capacity for new learning and information processing in novel situations[84]. After excluding subjects with null or invalid scores, we selected 400 adolescents for subsequent analysis.

Construction of individualized homologous functional parcellations

Iterative functional registration of local gradient maps. The RSFC gradients reflect transitions in resting-state functional connectivity across the cortical surface, which can serve as boundaries in brain parcellations[85] and converged with other modalities, including task-evoked activity and cellular architecture boundaries[86]. Consequently, we first computed functional connectivity using the timeseries of vertices from the fs_LR_32k surface template, and transformed the results to z scores using Fisher's r-to-z transformation. Then, we obtained individual and population-averaged local gradient maps through a gradient-based parcellation technique by using "watershed by flooding" procedure with RSFC map similarity matrix (Fig. 2a and Supplementary Fig. 4a)[75,87,88].

Given the highly variable relationship between cortical folds and brain function, we employed a functional gradient-based registration to the population-average gradient. Specifically, individual gradient maps were co-registered to the population-average gradient map using cortical folding features through the Multimodal Surface Matching (MSM)[89]. These individual maps were then averaged to generate a new population-average gradient map. This process was iterated until the difference between two consecutive population-mean gradient maps was not statistically significant ($P > 0.05$) (Supplementary Fig. 4b). We selected the group-level gradient maps after 15th iterations for further analysis, as the variability between two consecutive iterations became nonsignificant beyond this point.

Task-constrained group parcellation maps. To improve the quality of individualized homologous functional parcellations (IHFPs), we constructed the age-specific and age-independent group parcellation maps as the prior information for IHFPs. We first incorporated task activation maps into the variant of gwMRF model[19], which integrates local gradient maps, global similarity, spatial connectedness and task activation maps to construct more precise group parcellation maps. The global similarity term ensures that brain regions with similar fMRI time courses are assigned to the same parcel, while the spatial connectedness term maintains spatial cohesion by keeping regions within a parcel close to its center. The local gradient term and task activation term contribute equally to penalizing differences in parcellation labels between neighboring regions. Data from all terms were reconstructed as an undirected connectivity graph, enabling fine-grained parcellations through graph cuts within a maximum-a-posteriori estimation framework.

To evaluate the performance after introducing task activation maps, we compared the task-related inhomogeneity of our group parcellations with those of Schaefer400[19]. We used three task measures from HCP-D, including the *Emotion*, *CARIT*, and *GUESSING* tasks. For each task measure, task-related inhomogeneity was measured by computing standard deviation of fMRI task activation (z-scores) within each parcel, and then averaged across all parcels. Subsequently, we performed task-constrained parcellation and gwMRF statistical analysis on the averaged inhomogeneity across all participants. Lower values indicate greater functional homogeneity. For demonstrating the individual variation, we also computed the intersubject functional variation, which quantifies difference in functional connectivity across participants and is corrected by regressing out the mean intrasubject variability[36].

Individualized homologous functional parcellations. We adopted the prominent model (cMS-HBM) to generate initial individual atlases, following the approach of Kong et al.[20], which can correspond well between the group priors and individual atlases. While group parcellations provide valuable prior information for estimating functional brain networks or parcels, they can obscure some individual network organization and information[14,20,27,70] and not guarantee functional homology across participants[24]. Thus, we establish an individualized functional homologous process to obtain IHFPs (Fig. 1a and Supplementary Fig. 2). We firstly calculated *similarity distribution masks* for each age group by overlapping areas across all individual parcellations, and then selected the mask regions by setting a threshold based on the local minimum of the stability distribution[3] to identify the central regions of homologous ROIs as the common reference[24]. *Reference parcellations* was obtained by spatially overlapping each age-independent group parcellation with its corresponding *similarity distribution mask*[24]. Individualized homologous functional parcellations were created through the areal matching process, which aligned individualized parcellations with corresponding *reference parcellation* based on their spatial overlaps on the cortical surface. Here, a priori assumption holds that a *reference parcellations* should roughly represent the center of the homologous parcels across different individuals. Thus, we used the group-level parcels as the common reference in matching parcels across individuals[24]. Parcellations with an overlap rate below 30% or fewer than four vertices were excluded. However, low spatial overlap between functional regions does not necessarily indicate that the discarded areas lack functional correspondence at their respective spatial locations. Therefore, we leverage the similarity of functional connectivity to compensate for the removal of regions with low overlap, thereby obtaining a more extensive and individualized brain parcellation during parcellation reassignment. Finally, we established the IHFPs and subsequent results of developmental trajectories which were visualized using the age-independent group-average parcellation maps.

There are several different approaches to evaluate the stability of parcellation[90]. In this study, we used Dice's coefficient[10,20,91] and NMI[3,92] to assess parcellation reliability. We compared the similarity of parcellation maps generated within-subjects (intrasubject, split-half timeseries of each subject) and those generated between different subjects (intersubject). Examples of individual parcellations derived from fMRI datasets were shown in Fig. 3a. We calculated parcel-wised Dice's coefficient with intrasubject and intersubject parcellations[19]. Then, the Dice's coefficient of each region was averaged across all participants to provide the visualizations of regional intersubject and intrasubject reproducibility. The distribution of NMI between intersubject and intrasubject was in the same way, measuring the reliability of IHFPs.

Construction of normative trajectories at areal- and network-level

Resting-state functional connectivity. For the 59,412 vertices in the fs_LR_32k space, functional connectivity matrices were computed for all vertex pairs. Negative FC values were set to zero[15]. To derive parcel-wise RSFC, vertex-wise RSFC values were averaged within each parcel. The global mean functional connectivity was then calculated by averaging RSFC across all parcels. Within-system functional connectivity was defined as the RSFC within each system, while between-system functional connectivity was calculated as the average RSFC between different parcels in different systems. Given that the functional connectivity can be leveraged as a key metric to characterize functional development[15], we employ it as a measure to delineate its developmental trajectory, providing novel insights into adolescent brain maturation.

Areal-level parcellations mapping to 17 networks. To examine developmental patterns of homologous parcellations within corresponding networks, IHFPs were mapped to the Yeo17 networks[26] across all participants (Supplementary Fig. 3). We firstly created the *binarized overlap matrix* between age-independent group-average parcellation

map and Yeo17 networks, assigning each parcel to the corresponding network with maximized cortical overlap. Winner-take-all parcel-to-network assignments can lead to homologous parcels being mapped to different networks across individuals based on IHFPs. Specifically, a parcel's second-best network match in one individual often aligns with the primary assignment of its homologous parcel in another individual. Given this inter-individual variability in parcel-to-network assignment patterns, we further generated the *alternate group alignment matrix* to perform subsequent network-level developmental analysis. We obtained group-level parcel-based connectome profiles by computing the vertex-wise RSFC matrix, averaging RSFC values within parcels defined by the task-constrained age-independent parcellation map, and then averaging each parcel-based connectome across individuals. In the same way, we calculated parcel-based connectome profiles at the individual level. Then, we calculated the similarity (eta^2) matrix[3] between group-level and individual-level parcel-wised connectome profiles across all participants. For each participant, we created *parcel-wised individual alignment matrix* by binarizing top 5% similarity matrix for each individual parcel and then assigning each individual parcel to corresponding networks through mapping the correspondence between each individual-level parcel and the group-level parcel to the possible network, which denote as *individualized alignment matrix*. We then averaged *individualized alignment matrix* to obtain matched probability matrix for each network across individuals. Finally, we set a threshold (92%) to create the *alternate group alignment matrix* and obtained the final alternate functional 17-networks (results across thresholds from 98% to 86% in 2% decrements are shown in Supplementary Fig. 9). Notably, the matched probability for the limbic network was lower than that of the other networks, and no parcels were assigned to the limbic network after applying the threshold (Fig. 4a). Moreover, the limbic network of the Yeo17 networks parcellation is located in a cortical region beneath the medial wall, characterized by a low SNR[38]. Consequently, we directed our subsequent analyses toward the remaining 16 networks[39].

Modeling normative trajectories for functional connectivity from childhood to adolescence. To model the normative growth curves across individuals, we employed the state-of-the-art GAMLSS model to predict the normative trajectories of functional connectivity[19,20,27]. The GAMLSS model first determines the optimal data distribution and parameters based on different criteria, and subsequently fits the developmental curves of brain functional features using these optimal parameters[15,27]. We implemented the GAMLSS framework, treating functional connectivity as the dependent variable and modeling age as a smooth predictor with a B-spline basis function to account for potential nonlinear developmental patterns. Sex and in-scanner head motion were incorporated as additional fixed effects and scanner sites as random effects. We adopted the Johnson's SU (JSU) family distributional assumption to ensure methodological consistency. We fitted ten GAMLSS models, specifying degrees of freedom (d.f. = 3–6) for the B-spline basis functions of the location (μ) parameters and default degrees of freedom (d.f. = 3–6) for the scale (σ) parameters. Consistent with prior studies, only an intercept was included for the ν and τ parameters. Model estimation employed a log-likelihood convergence threshold of 0.001, with a maximum of 100 iterations. The best-fitting model for each functional metric was selected based on the lowest Bayesian Information Criterion (BIC) among all models that achieved convergence.

The strength of the developmental trajectories of global mean functional connectivity was defined as the 50th percentile at each age, with the growth rate quantified as the first derivative of this trajectory across ages (Fig. 3c, d). In addition, we calculated the strength and growth rate of within-system and between-system functional connectivity trajectories across all ages (Supplementary Figs. 6–7). For network-level normative trajectories, we conducted the weighted average of the global mean functional connectivity for parcellations within each network, with weights derived from

the group alignment matrix. The normative trajectories for each network were fitted using the GAMLSS model and subsequently plotted from childhood to adolescence (Fig. 4b). To examine the normative trajectories constructed using the alternative functional 17-network parcellation derived from IHFPs, we also conducted comparative analyses with the traditional group-level Yeo 17-network parcellation. In addition, we estimated the growth rates of the developmental trajectories for each network by bootstrapping 500 iterations, defining growth rate as the derivative of the 50th percentile trajectory (Supplementary Fig. 10). We further computed age-related difference curves comparing the 50th percentile growth rates between the IHFP-derived alternative parcellation and the canonical Yeo 17-network parcellation.

Variability of normative trajectories within each network. To assess the variability of areal-level normative trajectories of global mean functional connectivity within each network, we calculated the mean absolute deviation (MAD) between each parcel's developmental curve and its corresponding network's developmental curve, regressed out the number of parcels assigned to each network. Variability was visualized by sorting the MAD values of all parcels in ascending order and plotting the centile scores (Fig. 4c). The MAD was computed using the following formula:

$$\Delta_p(n) = E|Y_p - V_n|,$$

where Y_p represents the areal-level normative trajectory of parcel p, and V_n represents the network-level normative trajectory of network n.

Application of functional connectome derived by IHFPs in prediction of cognitive behavioral measures
Prediction of behavioral measures. We employed kernel ridge regression (KRR)[78] to predict individual behaviors in the HCP-D dataset, leveraging functional features derived from IHFPs and the Kong2021 atlas[20]. A 10-fold ridge regression analysis was performed on behavioral data from 400 selected participants, with head motion, age, and sex controlled during prediction[40]. Predictive features were generated using the Kong2021 and IHFPs for behavioral measures, including within-system and between-system functional connectivity.

Feature generalization across behavioral measures. Based on the behavioral prediction results, we applied the Haufe transformation[93] to create a predictive performance matrix for the functional features, where both positive and negative values indicated the relevance of these features in predicting behavioral measures.

Statistics and reproducibility
To test the robustness of our findings after controlling for sample size, epoch number, scanning duration, head motion and scanner site across age groups, we constructed a balanced dataset (Supplementary Table 1). In the balanced dataset, group-level gradient maps, group parcellations, and individual parcellations were constructed using the same procedures used for the discovery cohort. Subsequently, individualized homologous parcellations were generated using an IHFP process by first aligning individualized parcellations with corresponding *reference parcellation* based on their spatial overlaps on the cortical surface, followed by realignment of non-overlapping functional regions according to the similarity of their functional connectivity. Developmental trajectories were then modeled at the areal-level using GAMLSS, with model parameters held consistent with those derived from the discovery cohort. Developmental trajectories from the balanced dataset and the discovery cohort allowed us to assess whether variations in age group sample sizes and scanner sites influenced the final conclusions.

Statistical significance for the comparison of task-related inhomogeneity between the original gwMRF and our task-constrained gwMRF, as

well as for the prediction performance of behavioral measures between Kong2021 and IHFP atlases using kernel ridge regression, was assessed using a two-tailed paired *t*-test.

Reporting summary

Further information on research design is available in the Nature Portfolio Reporting Summary linked to this article.

Data availability

The Human Connectome Project Development data is available for download through the NIMH Data Archive (https://nda.nih.gov/). The source data generated in this study, along with the selected participants' IDs from the HCP-D dataset, are deposited on our GitHub page (https://github.com/BIT-YangLab/IHFPs). The source data behind the graphs in the paper can be found in Supplementary Data 1.

Code availability

The code for analyzing the data can be found on our GitHub page (https://github.com/BIT-YangLab/IHFPs). The postprocessing procedure for fMRI uses the published pipelines available at https://github.com/ThomasYeoLab/CBIG/tree/master/stable_projects/preprocessing/CBIG_fMRI_Preproc2015. Code to generate task activation maps is provided at https://github.com/Washington-University/HCPpipelines. Code for performing local gradient maps is available at https://github.com/MidnightScanClub. The code for gwMRF can be found at https://github.com/ThomasYeoLab/CBIG/tree/master/stable_projects/brain_parcellation/Schaefer2018_LocalGlobal. Additional tools used to work with CIFTI files that were used to support the findings for this study were as follows: MSM v3.0 (https://github.com/ecr05/MSM_HOCR), Connectome Workbench v1.5.0 (https://www.humanconnectome.org/software/connectome-workbench), R v4.4.1 (https://www.r-project.org), and GAMLSS package v5.4–3 (https://www.gamlss.com/).

References

1. Eickhoff, S. B., Yeo, B. T. & Genon, S. Imaging-based parcellations of the human brain. *Nat. Rev. Neurosci.* **19**, 672–686 (2018).
2. Lawrence, R. M. et al. Standardizing human brain parcellations. *Sci. Data* **8**, 78 (2021).
3. Hermosillo, R. J. et al. A precision functional atlas of personalized network topography and probabilities. *Nat. Neurosci.* **27**, 1000–1013 (2024).
4. Dworetsky, A. et al. Two common and distinct forms of variation in human functional brain networks. *Nat. Neurosci.* **27**, 1187–1198 (2024).
5. Nettekoven, C. et al. A hierarchical atlas of the human cerebellum for functional precision mapping. *Nat. Commun.* **15**, 8376 (2024).
6. Yang, G. et al. Global diversity in individualized cortical network topography. *Cereb. Cortex* **33**, 6803–6817 (2023).
7. Cui, Z. et al. Linking individual differences in personalized functional network topography to psychopathology in youth. *Biol. Psychiatry* **92**, 973–983 (2022).
8. Keller, A. S. et al. Personalized functional brain network topography is associated with individual differences in youth cognition. *Nat. Commun.* **14**, 8411 (2023).
9. Lynch, C. J. et al. Frontostriatal salience network expansion in individuals in depression. *Nature* **633**, 624–633 (2024).
10. Persichetti, A. S., Shao, J., Gotts, S. J. & Martin, A. A functional parcellation of the whole brain in high-functioning individuals with autism spectrum disorder reveals atypical patterns of network organization. *Mol. Psychiatry* **30**, 1518–1528 (2024).
11. Tervo-Clemmens, B. et al. A canonical trajectory of executive function maturation from adolescence to adulthood. *Nat. Commun.* **14**, 6922 (2023).
12. Dong, H.-M. et al. Ventral attention network connectivity is linked to cortical maturation and cognitive ability in childhood. *Nat. Neurosci.* **27**, 2009–2020 (2024).
13. Sanders, A. F. et al. Age-related differences in resting-state functional connectivity from childhood to adolescence. *Cereb. Cortex* **33**, 6928–6942 (2023).
14. Cui, Z. et al. Individual variation in functional topography of association networks in youth. *Neuron* **106**, 340–353.e348 (2020).
15. Sun, L. et al. Human lifespan changes in the brain's functional connectome. *Nat. Neurosci.* **28**, 891–901 (2025).
16. Tooley, U. A. et al. The age of reason: functional brain network development during childhood. *J. Neurosci.* **42**, 8237–8251 (2022).
17. Glasser, M. F. et al. A multi-modal parcellation of human cerebral cortex. *Nature* **536**, 171–178 (2016).
18. Sydnor, V. J. et al. Neurodevelopment of the association cortices: Patterns, mechanisms, and implications for psychopathology. *Neuron* **109**, 2820–2846 (2021).
19. Schaefer, A. et al. Local-global parcellation of the human cerebral cortex from intrinsic functional connectivity MRI. *Cereb. Cortex* **28**, 3095–3114 (2018).
20. Kong, R. et al. Individual-specific areal-level parcellations improve functional connectivity prediction of behavior. *Cereb. Cortex* **31**, 4477–4500 (2021).
21. Wang, S., Tepfer, L. J., Taren, A. A. & Smith, D. V. Functional parcellation of the default mode network: a large-scale meta-analysis. *Sci. Rep.* **10**, 16096 (2020).
22. Braga, R. M. & Buckner, R. L. Parallel interdigitated distributed networks within the individual estimated by intrinsic functional connectivity. *Neuron* **95**, 457–471.e455 (2017).
23. Gao, C. et al. Individualized brain mapping for navigated neuromodulation. *Chin. Med. J.* **137**, 508–523 (2024).
24. Li, M. et al. Performing group-level functional image analyses based on homologous functional regions mapped in individuals. *PLoS Biol.* **17**, e2007032 (2019).
25. Yeo, B. T. et al. Functional specialization and flexibility in human association cortex. *Cereb. cortex* **25**, 3654–3672 (2015).
26. Thomas Yeo, B. et al. The organization of the human cerebral cortex estimated by intrinsic functional connectivity. *J. Neurophysiol.* **106**, 1125–1165 (2011).
27. Kong, R. et al. Spatial topography of individual-specific cortical networks predicts human cognition, personality, and emotion. *Cereb. Cortex* **29**, 2533–2551 (2019).
28. Wang, F. et al. Fine-grained functional parcellation maps of the infant cerebral cortex. *elife* **12**, e75401 (2023).
29. Tu, J. C. et al. Early life neuroimaging: The generalizability of cortical area parcellations across development. *bioRxiv*, 2024.09.09.612056 (2024).
30. Glasser, M. F. et al. The minimal preprocessing pipelines for the Human Connectome Project. *Neuroimage* **80**, 105–124 (2013).
31. Bethlehem, R. A. et al. Brain charts for the human lifespan. *Nature* **604**, 525–533 (2022).
32. Stasinopoulos, D. M. & Rigby, R. A. Generalized additive models for location scale and shape (GAMLSS) in R. *J. Stat. Softw.* **23**, 1–46 (2008).
33. Borghi, E. et al. Construction of the World Health Organization child growth standards: selection of methods for attained growth curves. *Stat. Med.* **25**, 247–265 (2006).
34. Li, H. et al. Spatial heterogeneity and subtypes of functional connectivity development in youth. *bioRxiv*, 2025.2001.2024.634828 (2025).

35. Sydnor, V. J. et al. Intrinsic activity development unfolds along a sensorimotor–association cortical axis in youth. *Nat. Neurosci.* **26**, 638–649 (2023).

36. Mueller, S. et al. Individual variability in functional connectivity architecture of the human brain. *Neuron* **77**, 586–595 (2013).

37. Harms, M. P. et al. Extending the human connectome project across ages: imaging protocols for the lifespan development and aging projects. *Neuroimage* **183**, 972–984 (2018).

38. Du, J. et al. Organization of the human cerebral cortex estimated within individuals: networks, global topography, and function. *J. Neurophysiol.* **131**, 1014–1082 (2024).

39. Chen, J. et al. Shared and unique brain network features predict cognitive, personality, and mental health scores in the ABCD study. *Nat. Commun.* **13**, 2217 (2022).

40. Kong, R. et al. Comparison between gradients and parcellations for functional connectivity prediction of behavior. *NeuroImage* **273**, 120044 (2023).

41. Yarkoni, T., Poldrack, R. A., Nichols, T. E., Van Essen, D. C. & Wager, T. D. Large-scale automated synthesis of human functional neuroimaging data. *Nat. Methods* **8**, 665–670 (2011).

42. Tulsky, D. S. et al. NIH Toolbox Cognition Battery (NIHTB-CB): List sorting test to measure working memory. *J. Int. Neuropsychol. Soc.* **20**, 599–610 (2014).

43. Cao, M. et al. Topological organization of the human brain functional connectome across the lifespan. *Dev. Cogn. Neurosci.* **7**, 76–93 (2014).

44. Betzel, R. F. et al. Changes in structural and functional connectivity among resting-state networks across the human lifespan. *Neuroimage* **102**, 345–357 (2014).

45. Tzourio-Mazoyer, N. et al. Automated anatomical labeling of activations in SPM using a macroscopic anatomical parcellation of the MNI MRI single-subject brain. *Neuroimage* **15**, 273–289 (2002).

46. Rolls, E. T., Joliot, M. & Tzourio-Mazoyer, N. Implementation of a new parcellation of the orbitofrontal cortex in the automated anatomical labeling atlas. *Neuroimage* **122**, 1–5 (2015).

47. Rolls, E. T., Huang, C.-C., Lin, C.-P., Feng, J. & Joliot, M. Automated anatomical labelling atlas 3. *Neuroimage* **206**, 116189 (2020).

48. Satterthwaite, T. D., Xia, C. H. & Bassett, D. S. Personalized neuroscience: common and individual-specific features in functional brain networks. *Neuron* **98**, 243–245 (2018).

49. Gratton, C. et al. Functional brain networks are dominated by stable group and individual factors, not cognitive or daily variation. *Neuron* **98**, 439–452.e435 (2018).

50. Wang, D. et al. Parcellating cortical functional networks in individuals. *Nat. Neurosci.* **18**, 1853–1860 (2015).

51. Miranda-Dominguez, O. et al. Connectotyping: model based fingerprinting of the functional connectome. *PloS One* **9**, e111048 (2014).

52. Anderson, K. M. et al. Heritability of individualized cortical network topography. *Proc. Natl. Acad. Sci. USA* **118**, e2016271118 (2021).

53. Gordon, E. M., Laumann, T. O., Adeyemo, B. & Petersen, S. E. Individual variability of the system-level organization of the human brain. *Cereb. Cortex* **27**, 386–399 (2017).

54. Dworetsky, A. et al. Probabilistic mapping of human functional brain networks identifies regions of high group consensus. *Neuroimage* **237**, 118164 (2021).

55. Doucet, G. E., Lee, W. H. & Frangou, S. Evaluation of the spatial variability in the major resting-state networks across human brain functional atlases. *Hum. Brain Mapp.* **40**, 4577–4587 (2019).

56. Fair, D. A. et al. Functional brain networks develop from a "local to distributed" organization. *PLoS Comput. Biol.* **5**, e1000381 (2009).

57. Tooley, U. A., Bassett, D. S. & Mackey, A. P. Functional brain network community structure in childhood: unfinished territories and fuzzy boundaries. *NeuroImage* **247**, 118843 (2022).

58. He, T. et al. Deep neural networks and kernel regression achieve comparable accuracies for functional connectivity prediction of behavior and demographics. *NeuroImage* **206**, 116276 (2020).

59. Ooi, L. Q. R. et al. Comparison of individualized behavioral predictions across anatomical, diffusion and functional connectivity MRI. *NeuroImage* **263**, 119636 (2022).

60. Nostro, A. D. et al. Predicting personality from network-based resting-state functional connectivity. *Brain Struct. Funct.* **223**, 2699–2719 (2018).

61. Xia, C. H. et al. Linked dimensions of psychopathology and connectivity in functional brain networks. *Nat. Commun.* **9**, 3003 (2018).

62. Tucker-Drob, E. M. et al. A strong dependency between changes in fluid and crystallized abilities in human cognitive aging. *Sci. Adv.* **8**, eabj2422 (2022).

63. Growney, C. M. & English, T. Fluid and crystallized cognitive resources differentially linked to emotion regulation success in adulthood. *Emotion* **23**, 589 (2023).

64. Hülür, G., Gasimova, F., Robitzsch, A. & Wilhelm, O. Change in fluid and crystallized intelligence and student achievement: The role of intellectual engagement. *Child Dev.* **89**, 1074–1087 (2018).

65. Dhamala, E., Jamison, K. W., Jaywant, A., Dennis, S. & Kuceyeski, A. Distinct functional and structural connections predict crystallised and fluid cognition in healthy adults. *Hum. Brain Mapp.* **42**, 3102–3118 (2021).

66. Akshoomoff, N. et al. VIII. NIH Toolbox Cognition Battery (CB): composite scores of crystallized, fluid, and overall cognition. *Monogr. Soc. Res. Child Dev.* **78**, 119–132 (2013).

67. Di Biase, M. A. et al. Mapping human brain charts cross-sectionally and longitudinally. *Proc. Natl. Acad. Sci. USA* **120**, e2216798120 (2023).

68. Casey, B. J. et al. The adolescent brain cognitive development (ABCD) study: imaging acquisition across 21 sites. *Dev. Cogn. Neurosci.* **32**, 43–54 (2018).

69. Rajimehr, R. et al. Functional architecture of cerebral cortex during naturalistic movie watching. *Neuron* **112**, 4130–4146.e4133 (2024).

70. Bell, P. T. & Shine, J. M. Subcortical contributions to large-scale network communication. *Neurosci. Biobehav. Rev.* **71**, 313–322 (2016).

71. Cummings, J. L. & Benson, D. F. Subcortical dementia: review of an emerging concept. *Arch. Neurol.* **41**, 874–879 (1984).

72. Mori, E. Impact of subcortical ischemic lesions on behavior and cognition. *Ann. N. Y. Acad. Sci.* **977**, 141–148 (2002).

73. Somerville, L. H. et al. The lifespan human connectome project in development: a large-scale study of brain connectivity development in 5–21 year olds. *Neuroimage* **183**, 456–468 (2018).

74. Wu, X. et al. Heritability of functional gradients in the human subcortico-cortical connectivity. *Commun. Biol.* **7**, 854 (2024).

75. Gordon, E. M. et al. Three distinct sets of connector hubs integrate human brain function. *Cell Rep.* **24**, 1687–1695.e1684 (2018).

76. Siegel, J. S. et al. Data quality influences observed links between functional connectivity and behavior. *Cereb. Cortex* **27**, 4492–4502 (2017).

77. Glasser, M. F. et al. The human connectome project's neuroimaging approach. *Nat. Neurosci.* **19**, 1175–1187 (2016).

78. Li, J. et al. Global signal regression strengthens association between resting-state functional connectivity and behavior. *NeuroImage* **196**, 126–141 (2019).

79. Ge, J. et al. Increasing diversity in connectomics with the Chinese Human Connectome Project. *Nat. Neurosci.* **26**, 163–172 (2023).

80. Smith, S. M. et al. Advances in functional and structural MR image analysis and implementation as FSL. *Neuroimage* **23**, S208–S219 (2004).

81. Lombardo, D. & Kaufmann, T. Different patterns of intrinsic functional connectivity at the default mode and attentional networks predict

crystalized and fluid abilities in childhood. *Cereb. Cortex Commun.* **4**, tgad015 (2023).

82. Prat, C. S. & Just, M. A. Exploring the neural dynamics underpinning individual differences in sentence comprehension. *Cereb. Cortex* **21**, 1747–1760 (2011).

83. Prat, C. S., Mason, R. A. & Just, M. A. An fMRI investigation of analogical mapping in metaphor comprehension: the influence of context and individual cognitive capacities on processing demands. *J. Exp. Psychol. Learn., Mem. Cogn.* **38**, 282 (2012).

84. Johann, V., Könen, T. & Karbach, J. The unique contribution of working memory, inhibition, cognitive flexibility, and intelligence to reading comprehension and reading speed. *Child Neuropsychol.* **26**, 324–344 (2020).

85. Cohen, A. L. et al. Defining functional areas in individual human brains using resting functional connectivity MRI. *Neuroimage* **41**, 45–57 (2008).

86. Wig, G. S., Laumann, T. O. & Petersen, S. E. An approach for parcellating human cortical areas using resting-state correlations. *Neuroimage* **93**, 276–291 (2014).

87. Gordon, E. M. et al. Generation and evaluation of a cortical area parcellation from resting-state correlations. *Cereb. cortex* **26**, 288–303 (2016).

88. Gordon, E. M. et al. Precision functional mapping of individual human brains. *Neuron* **95**, 791–807.e797 (2017).

89. Robinson, E. C. et al. MSM: a new flexible framework for multimodal surface matching. *Neuroimage* **100**, 414–426 (2014).

90. Moghimi, P. et al. Evaluation of functional MRI-based human brain parcellation: a review. *J. Neurophysiol.* **128**, 197–217 (2022).

91. Dice, L. R. Measures of the amount of ecologic association between species. *Ecology* **26**, 297–302 (1945).

92. Danon, L., Diaz-Guilera, A., Duch, J. & Arenas, A. Comparing community structure identification. *J. Stat. Mech.Theory Exp.* **2005**, P09008 (2005).

93. Haufe, S. et al. On the interpretation of weight vectors of linear models in multivariate neuroimaging. *Neuroimage* **87**, 96–110 (2014).

Author contributions
G.Y., T.Y., and J.L. designed research; J.L. analyzed the data; J.L. and G.Y. wrote the first draft of the manuscript; J.L., Y.Z., X.W., M.X., Z.W., S.L., R.Y., W.Z., X.L., T.Y., and G.Y. edited the manuscript.

Competing interests
The authors declare no competing interests.

Additional information
Supplementary information The online version contains supplementary material available at https://doi.org/10.1038/s42003-025-08509-7.

Correspondence and requests for materials should be addressed to Tianyi Yan or Guoyuan Yang.

Peer review information *Communications Biology* thanks Attakias T. Mertens, Lianglong Sun and the other, anonymous, reviewer(s) for their contribution to the peer review of this work. Primary Handling Editor: Jasmine Pan.

Reprints and permissions information is available at http://www.nature.com/reprints

Publisher's note Springer Nature remains neutral with regard to jurisdictional claims in published maps and institutional affiliations.